1 **Influence of oil saturation upon spectral induced polarization of oil**

2 **bearing sands**

3 M. Schmutz (1), A. Revil (2, 3), P. Vaudelet (1), M. Batzle (2), P. Femenía Viñao (2), and D. D.

4 Werkema (4)

5

6 (1) Institut EGID, Université Bordeaux 3, 33607 Pessac, France.
7 (2) Colorado School of Mines, Dept. of Geophysics, Golden, CO, USA.
8 (3) INSU-CNRS LGIT UMR 5559, Université de Savoie, Equipe Volcans, Le Bourget du Lac, France.
9 (4) U.S. EPA, ORD, NERL, ESD, CMB, Las Vegas, Nevada, USA .

10

11 **Running title:** IP signature of oil in sand
12 **Corresponding author:** André Revil (arevil@mines.edu)

13 Emails: arevil@mines.edu; mbatzle@mines.edu; pierre.vaudelet@gmail.com;

14 schmutz.myriam@gmail.com; werkema.d@epamail.epa.gov; elmeuhort@msn.com

15

16

17 *Intended for Publication in Geophysical Journal International*

18

1   **Abstract.** The induced polarization model developed recently by Revil & Florsch (2010) to model

2   the complex conductivity of fully saturated granular materials has been extended to partial saturation

3   conditions. It is an improvement over previous models like the Vinegar and Waxman model, which

4   do not account explicitly for the effect of frequency. The Vinegar and Waxman model can be

5   considered as a limiting case of the Revil and Florsch model in the limit where the distribution of

6   relaxation times is very broad. The extended model is applied to the case of unconsolidated sands

7   partially saturated with oil and water. Laboratory experiments were performed to investigate the

8   influence of oil saturation, frequency, grain size, and conductivity of the pore water upon the

9   complex resistivity response of oil bearing sands. The low-frequency polarization (below 100 Hz) is

10   dominated by the polarization of the Stern layer (the inner part of the electrical double layer coating

11   the surface of the grains in contact with water). The phase exhibits a well-defined relaxation peak

12   with a peak frequency that is dependent on the mean grain diameter as predicted by the model. Both

13   the resistivity and the magnitude of the phase increase with the relative saturation of the oil. The

14   imaginary (quadrature) component of the complex conductivity is observed to decrease with the oil

15   saturation. All these observations are reproduced by the new model.

16   **Keywords:** Complex resistivity, complex conductivity, induced polarization, oil.

1. Introduction

Induced polarization represents the measurement of the conductivity response (magnitude and phase) over a frequency range typically occurring from one milliHertz (sometimes down to the microhertz, see Olhoeft, 1985) to a few tens of kHz. Two electrodes are used to inject and retrieve the electrical current and two electrodes are used to measure the resulting difference of electrical potential and the phase lag between the current and the voltage (Marshall & Madden, 1959; Olhoeft, 1986; Sturrock 1999; Lesmes & Morgan 2001; and Slater & Lesmes 2002a). In addition to the classical applications of induced polarization to the prospection of ore bodies, this non-intrusive method has been used for environmental purposes, especially to investigate contaminant plumes (Olhoeft, 1986; Slater & Lesmes, 2002b) and to interpret downhole measurements in oil-bearing sediments (Vinegar & Waxman, 1982, 1984).

In the present study, we are interested in the effect of a non-wetting oil in the pore space of a porous sand upon the measurements of the spectral induced polarization. The presence of oil in porous materials has a characteristic electrical signature that depends on the amount of polar components in the oil and therefore depends on its wettability with respect to the solid phase (Olhoeft, 1986; Börner et al., 1993). Therefore the electrical signature of an oil-bearing sand also depends on the maturity of the oil or the time in which the oil has existed in the subsurface. This time dimension is one of the main factors controlling the biodegradation and the biogeophysical response of oil spills. Previous works have already shown that the induced polarization response of unsaturated porous materials changes with the saturation of the water phase (Vinegar & Waxman, 1982, 1984; Ulrich & Slater, 2004; Binley et al., 2005; Ghorbani et al., 2008). Olhoeft (1986) reported an increase of the phase of materials containing clay particles and contaminated with oil.

1   Vanhala *et al.* (1992) described the spectral induced polarization signature associated with the

2   presence of toluene, heptane, and ethylene glycol in glacial tills. They observed an increase of the

3   magnitude of the phase in the presence of these organic contaminants. Börner *et al*. (1993) observed

4   an increase of the magnitude of the phase in clays in the presence of organic contaminants and a

5   decrease of the magnitude of the phase for oil contaminated sandstones except in the case of

6   benzene. Vanhala (1997) showed that the introduction of motor oil decreases the magnitude of the

7   phase of glacial sediments (sands and tills). Recently, Cassiani et al. (2009) performed an

8   investigation showing the effect of the saturation in hydrocarbons upon induced polarization (using a

9   non-wetting oil) but they investigated only few extreme values in the oil saturation. They were able

10   to fit their data with the empirical Cole-Cole model but this empirical relationship does not explain

11   the experimental results from a mechanistic standpoint.

12   With the exception of the work of Vinegar & Waxman (1984), no quantitative model has

13   been developed to interpret the available experimental data and to see what fundamental mechanisms

14   could explain these experimental observations. Vinegar & Waxman (1984) were the first to develop

15   a model based on the polarization of the Stern layer plus the effect of membrane polarization.

16   However, they did not accounted for frequency dependence of the in-phase and quadrature

17   conductivities and therefore were not be able to explain experimental data showing peaks in the

18   phase lag or quadrature conductivity.

19   In the present investigation, we performed new laboratory experiments showing the influence

20   of oil saturation, grain size, and conductivity of the pore water upon the complex resistivity response

21   of oil bearing sands. In addition, we developed a quantitative and testable model to explain these

22   experimental results. This model is based on a description of the polarization of the electrical double

1 layer at the grain / water interface and is an extension of the model published recently by Revil and

2 Florsch (2010).

3

4 **2. Theoretical Background**

5

6 There exist numerous models describing the high-frequency electromagnetic properties of

7 partially saturated sedimentary rocks (e.g., Cappacioli *et al*., 2001). However, to the best of our

8 knowledge, the only quantitative model proposed in the literature to account for the effect of oil

9 saturation upon low frequency (< 100 Hz) complex conductivity measurements of partially saturated

10 sandstones is the model developed by Vinegar & Waxman (1982, 1984). A description of this model

11 is provided in Appendix A. However, this model does not account for the frequency dependence of

12 the in-phase and quadrature conductivities and therefore needs to be extended with that respect. We

13 will show that the Vinegar & Waxman (1982, 1984) model could be considered as the limiting case

14 of a model accounting explicitly for the grain size distribution.

15 Recently a new model has been developed by Revil & Florsch (2010) in terms of providing a

16 linear quantitative model for the low frequency complex conductivity of a partially saturated pack of

17 sand grains characterized by a median D_{50} and a standard deviation $\hat{\sigma}$. This model was developed to

18 relate quantitatively spectral induced polarization to permeability for fully water-saturated granular

19 media. It accounts explicitly for the grain size distribution through a polarization of the electrical

20 double layer coating the surface of the grains. At low frequencies (typically below 100 Hz), the main

21 induced polarization mechanism discussed by Revil & Florsch (2010) corresponds to the polarization

22 of the inner portion of the electrical double layer, the so-called Stern layer (Figure 1). The external

23 part of the electrical double layer only contributes to the DC conductivity and is considered to be

1 independent of the frequency. An additional mechanism, called Maxwell-Wagner polarization, is

2 also known to contribute at higher frequencies. While the electrical double layer polarization is due

3 to the accumulation of charge carriers at some discontinuities in the porous material (called

4 polarization length scales), the Maxwell-Wagner polarization is due to the discontinuity of the

5 current displacement at the interface between the different phases of the porous material. The

6 Maxwell-Wagner contribution is therefore dielectric in nature. This dielectric contribution can be

7 dominant above 1 kHz (e.g., Lesmes & Morgan, 2001; Leroy *et al*., 2008). In the present paper, we

8 are mainly interested in the low-frequency content of the induced polarization spectra for which the

9 Stern layer polarization seems to dominate, so we ignore the Maxwell-Wagner polarization effect

10 and we consider only our data in the frequency range 1 mHz-100 Hz because the effect of the

11 saturation upon the Maxwell-Wagner polarization is fairly well-known.

12   In a water saturated sand, the polarization of the Stern layer occurs because the Stern layer is

13 discontinuous at the scale of the representative elementary volume. Indeed, the grains are in contact

14 with each other but the grain-to-grain contiguity provides only a continuous pathway for the diffuse

15 layer that extends few nanometers to tens of nanometers in the pore space. The Stern layer formed by

16 the sorption of counterions (generally cations) on the mineral surface remains discontinuous at the

17 grain-to-grain contacts. In addition, we consider that sorption-desorption processes of the

18 counterions do not appear in the investigated frequency range (1 mHz-100 Hz). Therefore, when an

19 electrical field is applied to a grain, the electromigration of the weakly sorbed cations of the Stern

20 layer (moving in the direction of the electrical field) accumulate at the edge of the grain and back-

21 diffuse in their concentration gradients (Leroy et al., 2008, Revil and Florsch, 2010). This idea is not

22 new and is essentially the same as proposed by Schwarz nearly fiftty years ago (Schwarz, 1962).

23 Schwarz studied the polarization of a compact layer of counterions coating the surface of an

1   insulating sphere. He based his approach on the assumption that there is no exchange of ions

2   between the Stern and the diffuse layers or the pore water. He therefore assumed that the counterions

3   can only move tangentially along the surface of the grains. This assumption seems plausible as the

4   kinetics of sorption/desorption of ions in the Stern layer is very slow (typically several hours, see

5   discussion in Revil *et al.*, 1999, their Figure 7 and Li *et al.* 2010). We consider therefore that the

6   characteristic length scale associated with this polarization mechanism is related to the size of the

7   grains. In the model developed by Revil & Flosch (2010), the influence of a grain size distribution is

8   accounted for through the use of a convolution product (see also Lesmes & Morgan, 2001).

9   In the presence of a partially saturated oil sand with a non-wetting oil, the pore volume is

10   filled by two continuous and immiscible fluid phases, a wetting fluid and a non-wetting fluid. In the

11   present investigation, the wetting fluid is water (subscript *w*) and the non-wetting fluid is oil

12   (subscript o). We denote $s_w \in [0;1]$ the relative saturation of the water phase and $s_o = 1 - s_w$ is

13   therefore the oil relative saturation. A sketch of the distribution of the different phases in the

14   presence of a non-wetting oil is shown in Figure 2a. When oil is the non-wetting phase, the diffuse

15   layer coating the surface of the sand grains is supposed to stay continuous over a representative

16   elementary volume of the sand including at high oil saturation because oil is the non-wetting phase.

17   The situation would be very different for a wetting oil as the electrical response would be possibly

18   controlled by the properties of the electrical double layer at the oil/water interface rather than by the

19   properties of the solid/water interface (see Figure 2).

20   We denote $\omega = 2\pi f$ the angular frequency, f the frequency (in Hertz), and $i = (-1)^{1/2}$ the pure

21   imaginary number. The magnitude of the conductivity $|\sigma|$ and the phase lag φ are related to the real

22   (in-phase) and imaginary (out-of-phase or quadrature) components of the complex conductivity σ^*,

23   σ' and σ'' (expressed in S m^{-1}) by,

$$\sigma^* = |\sigma| \exp(i\varphi) = \sigma' + i\sigma'', \tag{1}$$

$$|\sigma| = \sqrt{\sigma'^2 + \sigma''^2}, \tag{2}$$

$$\tan\varphi = \sigma'' / \sigma'. \tag{3}$$

4 Induced polarization is usually displayed as a resistivity magnitude $|\rho| = 1/|\sigma|$ (in ohm m) and a

5 phase φ (in rad) or alternatively as in-phase and quadrature conductivities, σ' and σ'', respectively.

6 We will use both representations below because the quadrature conductivity is directly related to

7 surface conductivity while the phase angle depends on both the in-phase and quadrature

8 conductivities.

9 In the present paper, we do not account (1) for the Maxwell-Wagner polarization occurring at

10 higher frequencies (>100 Hz) and (2) the conductivity of the oil, which is assumed to be insulating

11 like the silica grains. As explained previously, the Stern layer is discontinuous at the scale of the

12 grains and therefore the relevant polarization length scale is the grain size. The diffuse layer is

13 continuous because it extends inside the pore space and therefore surrounds continuously all the

14 grains. The oil phase phase is assumed to be continuous and the oil-water interface is assumed to be

15 uncharged. Using the approach of Revil & Florsch (2010) (see also Leroy *et al.*, 2008 and Leroy &

16 Revil, 2009), the low-frequency complex electrical conductivity is written as (see Appendix B),

17

$$\sigma(\omega) = \frac{s_w^{\,n}}{F} \left[\sigma_w + \beta_{(+)} \frac{\overline{Q}_V}{s_w} + (F-1) \frac{\sigma_S(\omega)}{s_w} \right], \tag{4}$$

19 where,

$$\sigma_S(\omega) = 4E_h \Sigma^S \left(1 - \int_0^\infty \frac{g(\tau)}{1 + i\omega\tau} d\tau \right), \tag{5}$$

$$E_h = \int_0^{+\infty} f(D) d\ln D, \tag{6}$$

1
$$\int_0^\infty g(\tau)d\tau = 1, \tag{7}$$

2   and $F = \phi^{-m}$ is the electrical formation factor (m is called the cementation exponent and ϕ is the

3   connected porosity), n is the saturation exponent (also called the second Archie's exponent, Archie,

4   1942), the term $\beta_{(+)}\bar{Q}_V$ (in S m^{-1}) represents the surface conductivity associated with the excess of

5   charges in the pore water (the so-called diffuse layer contribution, see Revil *et al.*, 2005), $\bar{Q}_V$ (in C

6   m^{-3}) is the excess of charge per unit pore water volume due to the diffuse layer, $\beta_{(+)}$ (in m^2 s^{-1} V^{-1})

7   represents the mobility of the cations in the main pore space assumed to be the same in the bulk pore

8   water and in the Stern layer, σ_w is the conductivity of the pore water, σ_S is the equivalent

9   conductivity of the grains coated by the Stern layer (in S m^{-1}), $g(\tau)$ represents the probability

10 distribution of the relaxation times τ, E_h (in m^{-1}) is the expected value of the probability density

11 function $h(\eta)$, which is the probability density distribution of the inverse of the grain diameter $\eta =$

12 $1/D$ (D is the grain diameter) and $f(D)$ is the probability density of the grain diameter distribution

13 (see Revil & Florsh, 2010 for details). The assumption that the mobility is the same in the bulk pore

14 water and in the Stern layer should be considered with caution: This assumption may be valid for

15 counterions that are weakly sorbed in the Stern layer (like sodium that keeps its hydration shell in the

16 Stern layer) but obviously does not hold for counterions that are strongly sorbed on the mineral

17 surface. A discussion on this subject is provided in Revil & Florsch (2010).

18   The saturation dependence of Eq. (4) is consistent with the model and experimental data of

19 Vinegar & Waxman (1982, 1984) (see Appendix A for a check of the consistency between the two

20 models). However, the model of Vinegar & Waxman (1982, 1984) does not explicitly account for

21 the frequency dependence of the in-phase and quadrature conductivities and the influence of the

22 grain size distribution while our model accounts explicitly for these dependencies. The reason for

23 this discrepancy is the following: Vinegar & Waxman (1982, 1984) worked with rocks characterized

24 by a very broad distribution of heterogeneities that translate into a very broad distribution of

1 relaxation times. Therefore, the convolutive effect of the heterogeneity is responsible for the lack of

2 dependence of the in-phase and quadrature components of the conductivity with the frequency over a

3 quite broad frequency range. In our case, the distribution of the heterogeneities will mainly

4 controlled by a narrow grain size distribution and we will clearly see the peak in the phase associated

5 with the expected value of this distribution. As explained in Appendix A, our model can be

6 considered as an extension of the Vinegar & Waxman model accounting explicitly for the effect of

7 the frequency.

8 The so-called surface conductivity $\sigma_S(\omega) = \sigma_S{}'(\omega) + i\sigma_S{}''(\omega)$ associated with the Stern layer

9 shown in Figure 1 can be decomposed into a real component and a quadrature component,

10

$$\sigma_S{}'(\omega) = \sigma_S^\infty \left(1 - \int_0^\infty \frac{g(\tau)}{1+\omega^2\tau^2} d\tau \right), \tag{8}$$

11

$$\sigma_S{}''(\omega) = \sigma_S^\infty \int_0^\infty \frac{\omega\tau}{1+\omega^2\tau^2} d\tau, \tag{9}$$

12

$$\sigma_S^\infty = 4\Sigma^S E_h. \tag{10}$$

13

14 The grain size distribution of the sand that we will consider later in this paper is log normal,

15

$$f(D) = \frac{1}{\sqrt{2\pi}\hat{\sigma}} \exp\left[-\frac{(\ln D - \mu)^2}{2\hat{\sigma}^2} \right], \tag{11}$$

16

17 with $\hat{\sigma} = \ln\sigma_g$ and $\mu = \ln D_{50}$ are the standard deviation and the mean of the grain diameter natural

18 logarithm, respectively, σ_g is the geometric standard deviation, and D_{50} represents the median of

19 the grain size distribution. The median D_{50} (in m) is used as a measure of the average particle

20 diameter size for the granular material. The standard deviation is a measure of the dispersion about

21 the mean grain diameter for a given distribution. In this case, the expectation of the distribution of

1
2 the inverse of the grain size is given by,

3
$$E_h = \exp\left(\frac{1}{2}\hat{\sigma}^2 - \mu\right) = \frac{1}{D_{50}}\exp\left(\frac{1}{2}\hat{\sigma}^2\right).$$
(12)

4 For such a grain size distribution, the related distribution of the relaxation times is given by (Revil &

5 Florsch, 2010),

6
$$g(\tau) = \frac{1}{\sqrt{2\pi}(2\hat{\sigma})\tau}\exp\left[-\left(\frac{\ln(\tau/\tau_0)}{\sqrt{2}(2\hat{\sigma})}\right)\right].$$
(13)

7 Note that the standard deviation for the distribution of the relaxation times is $2\hat{\sigma}$ and not $\hat{\sigma}$. In the

8 model developed by Schwartz (1962), the relaxation time for an ion of species i, τ_0 (in s), is therefore

9 related to the diffusion coefficient of the ion i in the Stern layer D_S^i by,

10
$$\tau_0 = \frac{\alpha D_{50}^2}{8D_S^i}.$$
(14)

11 where $\alpha = F\phi$ is the tortuosity given by the product of the formation factor F with the connected

12 porosity ϕ. This tortuosity correction does not appear in the original paper of Schwartz (1962) and is

13 due to Binley *et al.* (2010). For the sands investigated in the present paper, the formation factor is 3.9

14 and the porosity is 0.4. This yields a bulk tortuosity equal to 1.56.

15 On a silica surface, surface conductivity is general very small with respect to the pore water

16 conductivity (except for very fresh pore waters). We assume conditions such as the conductivity

17 term associated with the pore water is larger than the surface conductivity term $(F-1)\sigma_S^\infty$. This

18 condition is satisfied for the tap water and is a quite good approximation for the demineralized water

19 used below in the experiments. Neglecting the contribution of the surface conductivity to the in-

20 phase conductivity, the in-phase and quadrature conductivities and the phase are given by,

21
$$\sigma' \approx \frac{S_w^n}{F}\sigma_w,$$
(15)

1

$$\sigma'' = -\frac{S_w^{\,n}}{F}\sigma_S^{\infty}(F-1)\frac{\omega\tau_0}{1+\omega^2\tau_0^{\,2}}, \tag{16}$$

2

$$\varphi = \mathrm{atan}\left[\frac{-\sigma_S^{\infty}(F-1)\dfrac{\omega\tau_0}{1+\omega^2\tau_0^{\,2}}}{s_w\sigma_w+(F-1)\sigma_S^{\infty}\left(1-\dfrac{1}{1+\omega^2\tau_0^{\,2}}\right)}\right], \tag{17}$$

3

$$\varphi \approx -\mathrm{atan}\left[\frac{\sigma_S^{\infty}(F-1)\omega\tau_0}{s_w\sigma_w\left(1+\omega^2\tau_0^{\,2}\right)}\right], \tag{18}$$

4   respectively.

5   In our model, we do not consider polarization for the diffuse layer because we assume that it

6   forms a continuous phase through the porous material even at partial saturations as long as oil is the

7   non-wetting phase. In contrast, the Stern layer polarizes because it is discontinuous. However the

8   assumption that the polarization is entirely due to the Stern layer should be consider with caution as

9   other contributions, such as the membrane polarization, have not been considered yet from a

10   quantitative standpoint (see a short discussion in Leroy & Revil, 2009).

11   An alternative view of the problem is to consider the influence of the specific surface area, S,

12   upon the phase or the quadrature conductivities. It is generally admitted that the higher the specific

13   surface area, the higher the polarization and therefore the quadrature conductivity. The surface area

14   per pore volume ratio is related to the expectation E_h by:

15

$$\frac{S}{V_p} \approx \frac{6}{\phi}\frac{1}{E_h}, \tag{19}$$

16

$$\frac{S}{V_p} \approx \frac{6}{D_{50}\phi}\exp\left(\frac{1}{2}\hat{\sigma}^2\right), \tag{20}$$

1   where ϕ represents the connected porosity. Therefore the mean grain size, the standard deviation of

2   the grain size distribution, the connected porosity, and the surface to pore volume ratio are all

3   connected parameters through Eq. (19) or Eq. (20).

4   We note φ_0 the value of the phase at the relaxation frequency (in s^{-1}) defined by $\omega_0 = 1/\tau_0$

5   where τ_0 is given by Eq. (14). Note that the relaxation occurs at a frequency that is, in principle;

6   independent on the saturation of the water phase. As successfully explained by Jougnot *et al.* (2010)

7   for clay-rocks (argillites), the effect of the saturation upon the phase is due to the fact that the

8   Maxwell-Wagner is not entirely negligible at the frequency at which the relaxation of the Stern layer

9   occurs. An alternative possibility would be that there is a small contribution from membrane

10 polarization that is saturation-dependent because occurring in the pore water phase and not along the

11 mineral surface. Using Eq. (18), this phase is given by,

12
$$\varphi_0 \approx -\frac{(F-1)\sigma_S^\infty}{2 s_w \sigma_w + (F-1)\sigma_S^\infty}. \tag{21}$$

13 Our model predicts therefore a change of the phase peak with the saturation. Using this high salinity

14 assumption, we obtain:

15
$$\varphi_0 \approx -\frac{\sigma_S^\infty (F-1)}{2 s_w \sigma_w}. \tag{22}$$

16 Using Eqs. (8) and (12) with the grain size distribution assumed to be described by a log normal

17 distribution, the high frequency surface conductivity is given by,

18
$$\sigma_S^\infty = \frac{2}{D_{50}} \Sigma^S \exp\left(\frac{1}{2}\hat{\sigma}^2\right), \tag{23}$$

19 and therefore the phase peak is given by,

20
$$\varphi_0 \approx -\frac{2\Sigma^S (F-1)}{\sigma_w D_{50}} \exp\left(\frac{1}{2}\hat{\sigma}^2\right) s_w^{-1}. \tag{24}$$

1   Neglecting the surface conductivity in the in-phase conductivity (for the brine saturated case), the in-

2   phase and quadrature conductivities at the phase peak are given by,

$$\sigma_0' \approx \frac{S_w^{\,n}}{F}\sigma_w, \tag{25}$$

$$\sigma_0'' = -\frac{S_w^{\,n-1}}{2F}\sigma_S^\infty(F-1). \tag{26}$$

5   Replacing the surface conductivity σ_S^∞ by its expression as a function of the specific surface

6   conductance, see Eq. (23), the quadrature conductivity peak can be written as,

$$\sigma_0'' = -\frac{1}{D_{50}}\left(\frac{F-1}{F}\right)\Sigma^S \exp\left(\frac{1}{2}\hat{\sigma}^2\right)S_w^{\,n-1}. \tag{27}$$

8   The sign "-" in this equation means that the phase lag between the current and the voltage is negative

9   (if the current is imposed, the voltage follows the current with a phase lag). These equations will be

10   tested below in Section 4.

11   A last point that is worth of discussion is the influence of the oil water interface upon

12   complex conductivity. In Figure 2, two end-members cases correspond to the cases of a pure non-

13   wetting oil and a pure wetting oil. In the first case, there are two interfaces to consider in principle in

14   the pore space: the grain/water interface and the oil/water interface. The model discussed above does

15   consider only the grain/water interface. This assumption is valid if the oil/water interface is non-

16   reactive and therefore does not form an electrical double layer in water or if the specific surface area

17   of the oil/water interface is much smaller than the specific surface area of the grain/water interface.

18   Experimental data shows however that there is an electrical double layer at the oil/water interface

19   including for non-wetting oils (*Volkov et al.*, 1996). However if the oil phase form a continuous

20   phase in the pore space of the porous material, we should not expect any polarization of the Stern

21   layer of the oil/water interface.

1   The case of a wetting oil should be quite different. Indeed, in the extreme case where oil

2   covers uniformly the surface of the grains, there is only one interface (the oil/water interface) and the

3   polar components contained in the oil (e.g., asphatenes) makes the oil/water interface quite reactive

4   in water and the setting of a strong electrical double layer. However this second case in not

5   investigated in the present paper and will be investigated in a separate contribution.

6

7   **3. Material and Methods**

8

9   As explained in Section 2, the spectral induced polarization method is based on the

10   measurements of the complex resistivity ρ^* (in ohm m) over several decades in frequency (in the

11   present case from 1 mHz to 45 kHz). The complex resistivity is the inverse of the complex

12   conductivity σ^*: $\rho^* = 1/\sigma^*$. What is actually measured is the complex resistance or impedance R^*

13   (in ohm) between the end-faces of a cylindrical sample for instance:

14
$$R^*(\omega) = \frac{U}{I} = \left|R^*(\omega)\right| e^{i\varphi(\omega)}, \tag{28}$$

15   where U is the measured voltage difference between electrodes M and N, which are called the

16   potential electrodes (see Figure 3), I the magnitude of the imposed current between the electrodes A

17   and B, which are called the current electrodes (Figure 3), and $\left|R^*(\omega)\right|$ and $\varphi(\omega)$ are the amplitude

18   and the phase of the complex impedance, respectively. The complex resistivity ρ^* is related to R^* by

19   a geometrical factor K (in m): $\rho^*(\omega) = KR^*(\omega)$. This geometrical factor K takes into account not

20   only the position of the electrodes in the tank but also the insulating boundary conditions at all

21   boundaries (Figure 3). The insulating boundary condition means that the normal component of the

22   current density and the electrical field are equal to zero at the boundaries. The geometrical factor was

1 calibrated by measuring the conductivity of the sand independently with a two-electrode device and

2 a cylindrical cell at 4 kHz (at this frequency, the polarization of the stainless steel electrodes can be

3 neglected). Note that the phase $\varphi(\omega)$ is the same for the resistivity and the impedance and is

4 independent on the value of the geometrical factor K.

5 To perform the experiments, we used a small tank filled with a mix of oil, water, and sand

6 grains (Figure 3). The amount of sand was kept the same and only the volumetric proportion of oil

7 and water was changed. A sketch of the experimental setup is shown in Figure 3. Both demineralized

8 and tap waters were used. The conductivity of the tap water was comprised between 1.20×10^{-2} S m^{-1}

9 and 1.70×10^{-2} S m^{-1} at 25°C. The electrical conductivity of the demineralized water was 5×10^{-4} S m^{-1}

10 at 25°C. The sand was a silica sand with the properties summarized in Table 1. The properties of

11 this sand were measured by Sakaki & Illangasekare (2007), and Sakaki (2009). We used two sands

12 denoted as Types A and B, respectively. Type A has a mean grain diameter of 200 μm while Type B

13 has a mean grain diameter of 500 μm.

14 All the experiments have been done under the same conditions, at ambient laboratory

15 temperatures, typically 24 ± 3 °C using exactly the same procedure. The composition of the tap

16 water is given in Table 2 (mass density 1000 kg m^{-3}). The light North Sea oil has a mass density of

17 898 kg m^{-3}. Its composition is reported in Table 3. So the difference in mass density between water

18 and oil is quite small. The plastic tank used for the experiments has a height of 8 cm, a length of

19 15cm, and a width of 10 cm.

20 The spectral induced polarization measurements were conducted using a ZEL-SIP04

21 impedance-meter developed at the Forschungszentrum, Juelich, Germany by Egon Zimmerman. The

22 characteristics of this apparatus including its accuracy and reliability were described extensively by

23 Zimmerman *et al.* (2008) and are not repeated here. An additional test can be found in Jougnot *et al.*

1   (2009). The sensitivity of this apparatus is typically at 0.1 mrad over most of the investigated

2   spectrum. A test reported in Jougnot *et al.* (2009) using a pure carbonate rock sample show no phase

3   as expected for this type of material.

4   At a room temperature of 24 ± 3 °C, measurements comprise 25 sinusoidal signals at various

5   frequencies, three measurements per decade, and the measurements are log-spaced in the frequency

6   range from 1 mHz to 45 kHz. Current was driven at the current electrodes A and B (Figure 3) by a

7   potential difference of 5 V. Both $Cu/CuSO_4$ (home-made) and $Pb/PbCl_2$ (Petiau electrodes,

8   manufactured by Geonesis in France) had been tested. The $Cu/CuSO_4$ electrodes have a 12 mm

9   diameter porous ceramic with a pore mean diameter of 2 μm and a hydraulic conductivity of 2.2×10^{-9}

10 m s^{-1}. The electrodes are made by a 10 cm length flexible plastic tube filled with $CuSO_4$ solution in

11 which a 10 cm length copper wire (diameter of 1mm) is inserted.

12   All the measurements performed with the non-wetting oil have been done with both types of

13 electrodes to compare the results. We found that (1) the experimental data were very similar,

14 especially in low frequency range from 10 mHz to 500 Hz and (2) accurate measurements could not

15 always be achieved in the very low frequency range (1 to 10 mHz) with the $Cu/CuSO_4$ electrodes

16 because of leakages of the copper sulfate solution in the tank generating sometimes instable

17 readings. Therefore only the Petiau electrodes were used in the entire frequency range from 1 mHz

18 to 45 kHz and are shown below. We used a square array of electrodes with AB=MN=AM=BN=7 cm

19 because it was the easiest electrode array to use with our tank geometry. However the response

20 should be independent of the selection of the electrode array as the sand in the sandbox is

21 homogeneously distributed.

22   For all the experiments, the preparation of adequate quantities of sand, oil, and water was

23 performed about 30 minutes before the beginning of the measurements. We mixed the different

1   components in the box shown in Figure 3. We first mixed oil with water and then the oil/water

2   mixture was mixed together with the sand. The same amount of sand was used for all the

3   experiments. At saturation with water, the porosity was estimated from the volume of the box, the

4   mass of the sand, and the density of silica (2650 kg m^{-3}). The measured porosity is 0.40±0.02. The

5   electrodes were inserted in the oil/sand/water mixture at a precise depth of 2 cm ± 1 mm (Figure 3).

6   The duration of a complete cycle of measurements was 90 minutes, most of the time required to do

7   the measurements being used to perform the measurements at lowest frequencies. Except when

8   shown on the figures, the estimated phase uncertainty was 0.1 mrad based on the tests reported in

9   Zimmerman *et al.* (2008).

10   A typical plot of the phase versus the frequency is shown in Figure 4. A clear relaxation can

11   be observed at low frequency and this relaxation is usually considered to be due to the polarization

12   of the electrical double layer coating the sand grains (see Leroy *et al.*, 2008 for a complete modeling

13   of this contribution in sands). At high frequencies (>100 Hz), the phase increases because of the

14   Maxwell-Wagner polarization as discussed extensively by Leroy *et al.* (2008). In the present paper,

15   we are however interested in the low-frequency behavior and we will plot only the low frequency

16   range of the investigated frequency range.

17

18   **4. Experimental Results and Interpretation**

19

20   All spectral induced polarization phase curves show a peak at low frequencies (in the 0.001-

21   0.1 Hz range), consistent with results presented recently by Cassiani *et al.* (2009) who used a non-

22   wetting oil. The values of the phase angles and the resistivity at the peak of the relaxation are

23   reported in Table 4. Measurements were done at five different saturations: $s_w = 1$ (the pore space is

1   fully saturated with water), $s_w = 0.80$, $s_w = 0.60$, $s_w = 0.40$, and $s_w = 0.20$. In the case of the pore space

2   fully saturated by oil, it was impossible to inject current in the sand/oil mixture because of the high

3   resistivity of the oil (typically 10^9 ohm m).

4   Both the magnitude of the resistivity and the absolute value of the phase increases when the

5   water saturation decreases. The resistivity increased from 300 ohm m for $s_w = 1$ to 10,000 ohm m for

6    $s_w = 0.2$. The absolute value of the phase increased from 3.4 mrad for $s_w = 1$ to 14.5 mrad for $s_w = 0.2$

7   (Figure 5). We also observed a shift in the frequency of the peak from 100 mHz at $s_w = 1$ to 10 mHz

8   at $s_w = 0.2$.

9   In order to check the influence of the salinity of the pore water, we did four experiments at

10   two water saturations ($s_w = 0.4$ and 0.6) with two different types of pore waters (Figure 6). We used

11   tap water (conductivity varying from 1.20×10^{-2} S m^{-1} and 1.70×10^{-2} S m^{-1} at 21±1°C) and

12   demineralized water. We observed a slight shift of the peak of the polarization with the change in the

13   ionic strength (from 20 mHz with tap water to 50 mHz with demineralized water). This is consistent

14   with the fact that the peak of the phase is not expected to be very sensitive to the conductivity of the

15   pore water, see Eq. (14). The most dramatic change concerns the amplitude of the phase, which is

16   much stronger for demineralized water ($\varphi = 11.3$ mrad for $s_w = 0.6$ and ($\varphi = 12.3$ mrad for $s_w = 0.4$)

17   than for tap water (($\varphi = 5.7$ mrad for $s_w = 0.6$ and ($\varphi = 7.6$ mrad for $s_w = 0.4$). This is consistent with

18   the model developed by Revil & Florsch (2010) and explained by the salinity dependence of the

19   specific surface conductivity Σ^S .

20   In order to also check the influence of the grain size, we performed experiments at two

21   distinct water saturations ($s_w = 0.4$ and 0.6) for the two types of sands: type A (200 μm) and B (500

22   μm). The results are shown in Figure 7. The resistivities did not show a strong dependence with the

1 grain size at s_w =0.6 and at s_w = 0.4. The effect of grain size is associated with surface conductivity in

2 the electrical double layer surrounding the grains (Figure 1). The conductivity is given by,

$$\sigma = \frac{s_w^{\ n}}{F}\left[\sigma_w + (F-1)\frac{4\Sigma_S}{s_w D_{50}}\right], \tag{29}$$

4 We use the following values for the model parameters: D_{50} = 200 μm (Type A), D_{50} = 500 μm (Type

5 B), σ_w = (1.4±0.2) x 10^{-2} S m^{-1} (tap water), F = 3.9, Σ^S = 2x10^{-9} S (see below), and n=2.14 (see

6 below). For s_w =0.6, we find ρ(sand A) = 820 ohm m (measured ~850 ohm m) and ρ(sand B) = 827

7 ohm m (measured ~850 ohm m). For s_w =0.4, we find ρ(sand A) = 1939 ohm m (measured ~1600

8 ohm m) and ρ(sand B) = 1963 ohm m (measured ~1500 ohm m). So surface conductivity can be

9 neglected in the in-phase conductivity. It represents ~1% of the in phase conductivity response for

10 sands A and B for the pore waters used in the present study. Therefore the in phase conductivity is

11 unable to distinguish the two types of sands.

12 With the phase (or the quadrature conductivity), it is easier to distinguish the two types of sands

13 because there a strong shift in the maximum of the phase maxima can be observed (Figure 7). Type

14 A (200 μm) sand has a peak frequency occurring at higher frequencies than Type B sand (500 μm).

15 The measured peak of the (ordinary) frequency f_0 is in the range 60-100 mHz for type A at

16 saturation in water (Figures 5 and 8) and 2 to 6 mHz for sand B (see Figure 5). These results are

17 consistent with the fact that the peak of the frequency depends on the square of the grain size: the

18 larger the grain size, the smaller the frequency peak. According to our model, the relaxation

19 frequency (in Hertz) is defined as $f_0 = \omega_0 / 2\pi = 1/\tau_0 = 4D_S^i / (\pi \alpha D_{50}^{\ 2})$. Taking D_S^i = 2.5 x 10^{-9} m^2 s$^-$

20 ^{1} (Leroy *et al.*, 2008) and a tortuosity α = 1.56 (given as the product of the formation factor by the

21 connected porosity), the relaxation frequency is 51 mHz for Type A and 8 mHz for type B.

22 Therefore there is a fair agreement between the theory and the observations. Type A is also

1   characterized by phases that are higher than Type B. This is consistent with the fact that a pack of

2   small grains has a surface area higher than a pack of coarser grains (see discussion in Section 2).

3   In Figure 8, we mixed in equal volume Sand A (fine) and Sand B (coarse) and we measured

4   the complex conductivity of the mixture using the same procedure as before. The spectrum of the

5   phase is compared with the spectra obtained with Sand A and Sand B at full water saturation (see

6   Figure 8). At 100 Hz the phase is found to be exactly in between the phase of Sand A and Sand B.

7   The frequency peak of the mixture (~30-50 Hz) is observed to be closer to the frequency peak of

8   Sand A (60-100 mHz) than to the frequency peak of sand B (~1-6 mHz). These results are also

9   qualitatively in agreement with our model as the characteristic grain size of a multimodal distribution

10   is given by (Revil & Florsch, 2010),

11
$$\frac{1}{E_h} = \left(\int_0^{+\infty} f(D) d\ln D \right)^{-1}. \tag{30}$$

12   If we consider a mixture of two very narrow grain size distributions (described by two delta

13   functions), we can write (Revil & Florsch, 2010):

14
$$\frac{1}{E_h} = \frac{1}{f_f / D_f + f_c / D_c}, \tag{31}$$

15   where f_f is the volumetric fraction of fine grains of diameter D_f and f_c is the volumetric fraction

16   of coarse grains of diameter D_c. In our case $f_f = f_c = 1/2$, $D_f = 200$ μm, $D_c = 500$ μm. Using Eq.

17   (31), this yields $1/E_h = 286$ μm. Replacing D_{50} in the expression of the peak frequency by $1/E_h$, the

18   relaxation frequency (in Hertz) is given as $f_0 = 4 D_S^i E_h^2 / (\pi \alpha)$. This yields a relaxation frequency of

19   25 mHz in fair agreement with the observed frequency peak of the mixture (~30-50 Hz)

1   We come back now to the in phase conductivity. The small dependence of the electrical

2   conductivity with the grain size implies that surface conductivity can be neglected. Therefore,

3   according to Eq. (4), we can write,

$$\sigma = \frac{1}{F} s_w^{\ n} \sigma_w,$$ (32)

5   From Figure 9a, the formation factor can be determined experimentally as 275 ohm m divided by the

6   resistivity of the pore water. The conductivity of the pore water is $\sigma_w = (1.4 \pm 0.2) \times 10^{-2}$ S m^{-1}, so the

7   formation factor is 3.9. This is consistent with a porosity of 0.40 and a cementation exponent of 1.5.

8   The experimental data obey also the second Archie's law with a saturation exponent n equal to 2.14

9   (see Figure 9). Vinegar & Waxman (1984, Their Table 10) reported a mean value of the exponent

10   term equal to 2.06 for sandstones). We use the following power law relationship to fit the values of

11   the phase (at the frequency of the peak of the low-frequency relaxation) with the saturation:

$$\varphi_0 = a s_w^{\ -b}.$$ (33)

13   We find $a = -3.5 \pm 0.5$ mrad and the exponent term is $b = 0.89 \pm 0.10$. In the case of the exponent,

14   the theoretical value obtained in Section 2 (equation 22) is $b = 1$. According to our model, the

15   constant a is given by,

$$a = -\frac{2\Sigma^S (F-1)}{\sigma_w D_{50}} \exp\left(\frac{1}{2}\hat{\sigma}^2\right).$$ (34)

17   The formation factor is equal to $F = 3.9$ (see above). The conductivity of the pore water is $\sigma_w =$

18   $(1.4 \pm 0.2) \times 10^{-2}$ S m^{-1}. The mean diameter of the grains is $D_{50} = 200 \pm 10$ μm (see Table 1). With the

19   values of the standard deviation reported in Table 1 (corresponding to a very narrow grain size

20   distribution), the exponential term is very close to one (1.04 for sand A and closer to 1 for sand B).

21   The specific surface conductivity Σ^S found by Bolève $et\ al.$ (2008) is equal to 4×10^{-9} S at 25°C.

1   They used sodium chloride solutions. In the present case, the solution is dominated by the bivalent

2   cation Ca^{2+} in the pore water (see Table 2). The presence of bivalent counterions decreases by a

3   factor two the inner potential of the diffuse layer (Lorne *et al.*, 1999, their Figure 18) and therefore

4   the specific surface conductance. Therefore, we consider $\Sigma^S = 2 \times 10^{-9}$ S in Eq. (31) to determine the

5   value of the coefficient *a*. This yields *a* = -4.1±0.7 mrad. This value is consistent with the value

6   determined from the fit of the experimental data *a* = - 3.5 mrad (see above). So both coefficients *a*

7   and *b* can be predicted by the model.

8   Another way to represent the data is to plot the quadrature conductivity as a function of the

9   frequency or the water saturation. Some authors prefer this representation of the data as the

10   quadrature conductivity is independent of the in-phase conductivity while the phase angle depends

11   both on the in-phase and quadrature conductivities. However one can argue that the in-phase and

12   quadrature conductivities are not independent either as they depends on the same parameters

13   (formation factor, specific surface conductance). The results are shown in Figure 10. The quadrature

14   conductivity at the relaxation frequency (denoted with a subscript *m*) increases with the water

15   saturation.

16   $$\sigma_0 '' = c s_w^{\ p} ,$$ (35)

17

18   And according to our model, we have,

19   $$c = -\frac{1}{D_{50}} \left(\frac{F-1}{F} \right) \Sigma^S \exp \left(\frac{1}{2} \hat{\sigma}^2 \right),$$ (36)

20   and *p = n*-1. Using *n* equal to 2.14 (see above), the theoretical value predicted by our model is *p* =

21   1.14. Using *F* = 3.9 (see above), D_{50} = 200 μm, a narrow grain size distribution such as the

22   exponential term is equal to one, and $\Sigma^S = 2 \times 10^{-9}$ S, the theoretical value of *c* is equal to 1.6 x 10^{-5} S

1   m^{-1}. These values can be compared to the experimental values $p = 1.26$ (Figure 11) and $c = 1.3 \times 10^{-5}$

2    $S \, m^{-1}$ (Figure 10). There is again a good agreement between the theory and the experimental data.

3   Figure 10 shows the dependence of the normalized quadrature conductivity versus water

4   saturation for the sand filled with the non-wetting oil and water and for two sandstones investigated

5   by Vinegar & Waxman (1984). The normalization is done with respect to the value of the quadrature

6   conductivity at saturation of the water phase. Our results are consistent with those of Vinegar &

7   Waxman (1984). According to the model developed above and the model of Vinegar & Waxman

8   (1984), the exponent of this relationship is $p = n - 1$. As $n = 2.14$ for our sample and the mean of n is

9   equal to 2.06 for the samples investigated by Vinegar & Waxman (1984, their Table 10), we expect p

10    $= 1.14$ in our case and $p = 1.06$ in the case of the data reported by Vinegar & Waxman (1984). We

11   observe an exponent that is equal to 1.26 for our data. Vinegar & Waxman (1984, p. 1282) found $p =$

12   1.11 ± 0.17. Therefore, the agreement between our model and the experimental data is fairly good.

13

14   **5. Concluding Statements**

15

16   We have performed spectral induced polarization measurements with fresh oil bearing sands

17   investigating the influence of different parameters including (1) the oil saturation, (2) the

18   conductivity of the pore water, and (3) the mean grain diameter of the sand. Our goal was to extend

19   and to further test the spectral induced polarization model developed recently by Revil & Florsch

20   (2010). This model is based on the polarization of the Stern layer at the sand / water interface and the

21   polarization length scale is the size of the grains because of the discontinuity of the Stern layer

22   between grains. For a non-wetting oil, the absolute value of the phase increases with the oil

23   saturation and decreases with the salinity. An increase of the mean grain diameter shifts the peak

1 frequency at lower frequencies and decreases the value of the phase in a predictable way. All these

2 results obtained with the non-wetting oil can be reproduced with the extension of the Revil &

3 Florsch model except the broadness of the distribution of relaxation times which remains

4 unexplained. The explanation may be found in the membrane polarization that has not being

5 incorporated yet in our model or in mutual polarization effects between the grains that are not

6 captured by the convolution product (David Lesmes, personal communication 2010). The application

7 of the present model to in situ measurements will require the determination of the temperature

8 dependence of the in-phase and quadrature conductivities and the experimental results and

9 temperature dependence of surface conductivity shown by Vinegar & Waxman (1984) could be used

10 for this purpose. The change of chemistry and biochemistry of an oil undergoing biodegradation in

11 the subsurface would be probably reflected by a change in the time-lapse induced polarization

12 signature and wettability of the oil. This is something worth to investigate in future works.

13

References

Binley A., S. Kruschwitz, D. Lesmes and N. Kettridge, 2010. Exploiting the temperature effects on low frequency electrical spectra of sandstone: determination of effective diffusion path lengths. in press in Geophysics.

Binley A., Slater L., Fukes M. & Cassiani G., 2005. The relationship between frequency dependent electrical conductivity and hydraulic properties of saturated and unsaturated sandstone, *Water Resour. Res.*, **41**, 13, W12417.

Bolève, A., Crespy, A., Revil, A., Janod F. & Mattiuzzo J. L., 2007. Streaming potentials of granular media: Influence of the Dukhin and Reynolds numbers, *J. Geophys. Res.*, **112**, B08204, doi:10.1029/2006JB004673.

Börner, F., Gruhne M., and Schön J., 1993. Contamination indications derived from electrical properties in the low frequency range, *Geophysical Prospecting*, **41**, 83-98.

Cassiani, G, Kemna, A., and Villa, A., 2009. Spectral induced polarization for the characterization of free-phase hydrocarbon contamination of sediments, *Near Surface Geophysics*, **7**, 5-6, 547-562.

City of Golden, 2009. Water Quality Report, 8 pp.

Ghorbani, A., Cosenza, Ph., Ruy, S., Doussan C. & Florsch N., 2008. Noninvasive monitoring of water infiltration in a clay loamy soil using Spectral Induced Polarization, *Water Resources Research*, **44**, W08402, doi:10.1029/2007WR006114.

Jougnot D., Ghorbani A., Revil A., Leroy P., and Cosenza P., 2010. Spectral Induced Polarization of partially saturated clay-rocks: A mechanistic approach, *Geophysical Journal International*, **180**(1), 210-224, doi: 10.1111/j.1365-246X.2009.04426.x.

1 Leroy P., Revil A., Kemna A., Cosenza P., & Gorbani A., 2008. Spectral induced polarization of
2   water-saturated packs of glass beads, *Journal of Colloid and Interface Science*, **321** (1), 103-117.

3 Leroy, P. & Revil A., 2009. Spectral induced polarization of clays and clay-rocks, *Journal of
4   Geophysical Research*, **114**, B10202, doi:10.1029/2008JB006114.

5 Lesmes, D.P. & Morgan F.D., 2001. Dielectric spectroscopy of sedimentary rocks, *J. Geophy. Res.,*
6   **106** (B7) 13329-13346.

7 Li, Y., Yue Q., & Gao, B., 2010. Adsorption kinetics and desorption of Cu(II) and Zn(II) from
8   aqueous solution onto humic acid, *Journal of Hazardous Materials*, **178**, 455–461.

9 Lorne, B., Perrier, F., & Avouac J.P., 1999. Streaming potential measurements 1. Properties of the
10   electrical double layer from crushed rock samples, *J. Geophy. Res.*, **104**, B8, 17,857-17,877.

11 Linde, N., Jougnot D., Revil A., Matthaï S.K., Arora T., Renard D., & Doussan C., 2007. Streaming
12   current generation in two-phase flow conditions, *Geophysical Research Letters*, **34**(3), L03306,
13   doi: 10.1029/2006GL028878.

14 Marshall, D. J., & Madden T.R., 1959. Induced polarization, a study of its causes, *Geophysics*, **24**,
15   790–816.

16 Olhoeft, G. R., 1986, Direct detection of hydrocarbon and organic chemicals with ground-
17   penetrating radar and complex resistivity: Petroleum, hydrocarbons and organic chemicals in
18   ground water-Prevention, Detection, and Restoration, NWWA/API, Proceedings, 284–305.

19 Olhoeft, G. R., 1985. Low-frequency electrical properties, *Geophysics,* **50**, 2492-2503.

20 Revil A., 1999. Ionic diffusivity, electrical conductivity, membrane and thermoelectric potentials in
21   colloids and granular porous media: a unified model, *Journal of Colloid and Interface Science*,
22   **212**, 503-522.

1   Revil, A., Schwaeger, H., Cathles, L.M., & Manhardt P., 1999. Streaming potential in porous media.

2   2. Theory and application to geothermal systems, *Journal of Geophysical Research*, **104**(B9),

3   20,033-20,048.

4   Revil, A., Leroy P. & Titov K., 2005. Characterization of transport properties of argillaceous

5   sediments. Application to the Callovo-Oxfordian Argillite, *Journal of Geophysical Research*,

6   **110**, B06202, doi: 10.1029/2004JB003442.

7   Revil A., Linde N., Cerepi A., Jougnot D., Matthäi S., & Finsterle S., 2007. Electrokinetic coupling

8   in unsaturated porous media, *Journal of Colloid and Interface Science*, **313**(1), 315-327,

9   10.1016/j.jcis.2007.03.037.

10   Revil, A. & Florsch, N., 2010. Determination of permeability from spectral induced polarization in

11   granular media, *Geophysical Journal International*, **181**, 1480-1498, doi: 10.1111/j.1365-

12   246X.2010.04573.x.

13   Sakaki, T., & Illangasekare T. H., 2007. Comparison of height-averaged and point-measured

14   capillary pressure–saturation relations for sands using a modified Tempe cell, *Water Resour.*

15   *Res.*, **43**, W12502, doi:10.1029/2006WR005814.

16   Sakaki, T., 2009. Physical, hydraulic, and thermal properties of silica sands for laboratory

17   experiments, *Internal Report, Center for Experimental Study of Subsurface Environmental*

18   *Processes* (CESEP), Colorado School of Mines, Golden, Colorado.

19   Schwarz, G., 1962. A theory of the low-frequency dielectric dispersion of colloidal particles in

20   electrolyte solution, *Journal of Physical Chemistry,* **66**, 2636-2642.

21   Sen, P.N., Scala, C., & Cohen, M.H., 1981. A self-similar model for sedimentary rocks with

22   application to the dielectric constant of fused glass beads, *Geophysics*, **46**(5), 781-795.

1   Slater, L. & Lesmes D., 2002a. IP interpretation in environmental investigations, *Geophysics*, **67**(1),

2   77-88.

3   Slater, L. & Lesmes D., 2002b. Electrical-hydraulic relationships observed for unconsolidated

4   sediments, *Water Resources Research*, **38** (10), 1213.

5   Sturrock, J. T., 1999, *Predictions of Hydraulic Conductivity using Spectral Induced Polarizations*,

6   Ms Dissertation, Boston College.

7   Towle, J.N., Anderson, R.G., Pelton, W.H., Olhoeft, G.R., & Labrecque, D., 1986. Direct detection

8   of hydrocarbon contaminants using the induced polarization method, *Geophysics*, **51**, 2, 446-446.

9   Ulrich, C. & Slater L. D., 2004. Induced polarization measurements on unsaturated, unconsolidated

10   sands, *Geophysics*, **69**(3), 762– 771.

11   Vanhala, H., Soininen H., & Kukkonen I., 1992. Detecting organic chemical contaminants by

12   spectral-induced polarization method in glacial till environment, *Geophysics*, **57**, 1014–1017.

13   Vanhala, H., 1997. Mapping oil-contaminated sand and till with the spectral induced polarization

14   (SIP) method, *Geophys. Prospect.*, **45**, 303–326.

15   Vinegar, H.J., and M.H. Waxman, 1982. Method and apparatus for determining shaliness and oil

16   saturations in earth formations using induced polarization in the frequency domain, U.S. Patent

17   no. 4,359,687.

18   Vinegar, H.J., & Waxman M.H., 1984. Induced polarization of shaly sands, *Geophysics*, **49**, 1267–

19   1287.

20   Volkov A. G., Deamer D. W., Tanelian D. L., Markin V. S., 1996. Electrical double layer at the

21   oil/water interface, *Progress in Surface Science*, **53**, 1, 1-134.

22   Waxman, M. H. & Smits, L. J. M., 1968. Electrical conductivities in oil bearing shaly sands, *Soc.*

23   *Pet. Eng. J.*, **8**, 107–122.

1   Zimmermann, E., Kemna, A., Berwix, J., Glaas, W., Münch, H.M. & Huisman, J.A., 2008. A high-

2   accuracy impedance spectrometer for measuring sediments with low polarizability, *Meas. Sci.*

3   *Technol*., **19**, doi:10.1088/0957-0233/19/10/105603.

Appendix A. Comparison with the Vinegar and Waxman Model

The Vinegar & Waxman (1982, 1984) model was developed to determine the phase and the resistivity of oil-bearing sandstones partially saturated with non-wetting oils. In this model, the distribution of the relaxation times is considered to be very broad but it is not explicitly accounted for. Therefore, over a broad frequency range, the in-phase and quadrature conductivities are frequency independent. At the opposite, in our model the distribution of the relaxation times is explicitly taken into account through a convolution with the probability distribution of the inverse of the grain diameters. We show below that our model is, however, consistent with the equations developed by Vinegar & Waxman (1982, 1984) with the exception that our model accounts for the frequency dependence of the in-phase and quadrature conductivities with frequency.

From Eq. (4), the low-frequency electrical conductivity is given by,

$$\sigma = \frac{s_w^{\,n}}{F}\Big[\sigma_w + s_w^{-1}\big(\beta_{(+)}\overline{Q}_V + (F-1)\sigma_S\big)\Big]. \tag{A1}$$

Using a first order Taylor expansion of Archie's law for a pack of spherical grains characterized by a value of the cementation exponent equal to 1.5 (from the differential effective medium theory applied to purely spherical grains, see Sen 1981), the term (F-1) at high porosities is approximated by,

$$F - 1 = \frac{3}{2}\left(\frac{1-\phi}{\phi}\right) + ... \tag{A2}$$

The in-phase surface conductivity associated with the Stern layer is given by,

$$\sigma_S{}' = \frac{2}{3}\left(\frac{\phi}{1-\phi}\right)\beta_{(+)} f\, Q_V, \tag{A3}$$

where f is the fraction of surface conductivity due to the Stern layer ($0 \le f \le 1$), ($1 - f$) is the fraction of surface conductivity due to the diffuse layer, and the factor $2\phi/\left[3(1-\phi)\right]$ represents a conversion

1 factor to convert a charge per unit surface of the mineral to a charge per unit pore volume. In Eq.

2 (A3), Q_V represents the total charge per unit volume including the Stern and the diffuse layer

3 contributions. The charge density Q_V can be determined from the Cation Exchange Capacity (CEC,

4 expressed in C kg^{-3}) of the rock (Waxman & Smits, 1968):

5
$$Q_V = \rho_S \left(\frac{1-\phi}{\phi} \right) \text{CEC} ,$$
(A4)

6 where ρ_S is the mass density of the solid phase (in kg m^{-3}) and ϕ is the connected porosity. In

7 addition, we have $\bar{Q}_V = (1-f)Q_V$. Combining Eq. (A1) to (A3), the in-phase conductivity is given

8 by,

9
$$\sigma' = \frac{1}{F} s_w^{\;n} \left(\sigma_w + \frac{\beta_{(+)} Q_V}{s_w} \right),$$
(A5)

10 Eq. (A4) corresponds to the Waxman & Smits (1968) model. The quadrature conductivity is

11 assumed related to the quadrature conductivity of the surface conductivity by,

12
$$\sigma'' = \frac{(F-1) s_w^{\;n-1}}{F} \sigma_S{}'' .$$
(A6)

13 At high porosity, inserting Eq. (A2) into Eq. (A6), we have,

14
$$\sigma'' \approx \frac{3}{2} \frac{(1-\phi) s_w^{\;n-1}}{\phi F} \sigma_S{}'' .$$
(A7)

15 Assuming that,

16
$$\sigma_S{}'' = -\frac{2}{3} \left(\frac{\phi}{1-\phi} \right) \beta_{(+)} f \, Q_V ,$$
(A8)

17 and inserting Eq. (A8) into Eq. (A7), the quadrature conductivity is given by,

18
$$\sigma'' = -\frac{s_w^{\;n-1}}{F} \beta_{(+)} f Q_V .$$
(A9)

1 This can be compared with the quadrature conductivity model of Vinegar & Waxman (1984, their

2 Eq. 36),

$$\sigma'' = -\frac{S_w^{n-1}}{F}\lambda_a Q_V . \tag{A10}$$

4 A comparison between Eqs. (A9) and (A10) implies $\lambda_a = \beta_{(+)} f$. Taking $f = 0.84$ (see Revil &

5 Florsch, 2010), we obtain $\lambda_a = 4.3 \times 10^{-8}$ m^2 s^{-1} V^{-1} using the mobility of sodium in water (5.19×10^{-8}

6 m^2 s^{-1} V^{-1} at 25°C) and $\lambda_a = 4 \times 10^{-9}$ m^2 s^{-1} V^{-1} using the value of the mobility of sodium along the

7 mineral surface suggested by Revil (1999, his Table 1) (0.51×10^{-8} m^2 s^{-1} V^{-1} at 25°C). The value

8 given by Vinegar & Waxman (1982, 1984, their Table 5) is equal to $\lambda_a = 4 \pm 2 \times 10^{-9}$ m^2 s^{-1} V^{-1}.

9 However it would be presumptuous to conclude too quickly that the mobility of the counterions in

10 the Stern layer is necessarily ten times lower than in the bulk pore water. Vinegar & Waxman (1982,

11 1984) indicated that in addition to the polarization of the mineral surface, there is an additional

12 polarization mechanism called the membrane polarization effect, which is not included in our model.

13 In addition, our model would predict a distribution of relaxation times that is narrower than observed

14 in the experiment reported in the main text. This may point out that another hidden mechanism, like

15 membrane polarization, is at play.

Appendix B. Extension of the Revil and Florsch model

For a water-saturated sand, the model developed by Revil & Florsch (2010) can be recasted as,

$$\sigma(\omega) = \frac{1}{F}\left[\sigma_w + \beta_{(+)}\bar{Q}_V + (F-1)\sigma_S(\omega)\right]. \tag{B1}$$

The first term in brackets corresponds to the frequency-independent conductivity of the brine, the second term corresponds to the frequency-independent surface conductivity associated with the diffuse layer, and the third term corresponds to the frequency dependent surface conductivity term associated with the Stern layer. Extending this model for partial saturations requires making this model compatible with some well-known relationships. One of them is the second Archie's law when surface conductivity can be neglected. This law states that the inverse of the formation factor should be replaced by $(1/F)s_w{}^n$ at partial saturation s_w. When surface conductivity can be neglected, this yields,

$$\sigma = \frac{1}{F}s_w{}^n\sigma_w, \tag{B2}$$

where n is the second Archie's exponent. In addition, we know from electrokinetic measurements that the excess of charge per unit volume scales as $\bar{Q}_V / s_w$ for conditions of partial saturations (see Revil *et al.*, 2007 and Linde *et al.*, 2007). Assuming that the whole surface conductivity contribution follows the same dependence, we obtain the following equation at partial saturation,

$$\sigma(\omega) = \frac{s_w{}^n}{F}\left[\sigma_w + \beta_{(+)}\frac{\bar{Q}_V}{s_w} + (F-1)\frac{\sigma_S(\omega)}{s_w}\right]. \tag{B3}$$

1 **Table**

2 **Table 1.** Measured properties of the loosely compacted sands used in the present study (from Sakaki

3 & Illangasekare, 2007 and Sakaki, 2009). These measurements include the connected porosity ϕ, the

4 hydraulic conductivity at saturation K_s, the mean grain diameter D_{50}, and the standard deviation of

5 the log normal grain size distribution $\hat{\sigma}$.

Sand Type	ϕ (-)	K_s (10^{-3} m s^{-1})	D_{50} (mm)	$\hat{\sigma}$
Type B(#30)	0.42	1.16±0.09	0.5	0.2
Type A(#70)	0.42	0.141±0.15	0.2	0.3

6

7

8 **Table 2.** Composition of the tap water (from City of Golden, 2009) with the assumption that

9 hardness is due to Calcium. This yields a TDS of 245 ppm (~4.9x10^{-2} S m^{-1} at 25°C). Measurement

10 made in April-May 2009.

Substance	Concentration (mmol/l)
Ca^{2+}	0.95
K^+	0.09
Na^+	1.44
Cl^-	1.30
SO_4^{2-}	0.82
HCO_3^-	0.75
pH	8.4

11

1   **Table 3.** Composition of the oil (in wt %) used for the experiments.

Molecules	Weight fraction (%)
Butanes	0.0
Pentanes	0.0
Hexanes	0.0
Heptanes	0.3
Octanes	0.5
Nonanes	1.0
Decanes	1.4
Undecanes	1.9
Dodecanes	2.5
Tridecanes	3.1
Tetradecanes	3.7
Pentadecanes	4.1
Hexadecanes	3.7
Heptadecanes	3.8
Octadecanes	4.0
Nonadecanes	3.8
Eicosanes	3.8
Heneicosanes	3.3
Docosanes	3.0
Tricosanes	2.8
Tetracosanes	2.7
Pentacosanes	2.5
Hexacosanes	2.3
Heptacosanes	2.4
Octacosanes	2.2
Nonacosanes	2.2
Triacontanes	2.2
Untriacontanes	2.2
Dotriacontanes	1.8
Tritriacontanes	1.7
Tetratriacontanes	1.5
Pentatriacontanes	1.7
Hexatriacontanes	1.4
Heptatriacontanes	1.1
Octatriacontanes	1.0
Nonatriacontanes	1.0
Tetracontanes	1.0
C4O+	22.5
Total:	100.0

1   **Table 4.** Values of the phase and the modulus of the resistivity at the peak of the relaxation for a

2   sand (Type A) saturated by the non-wetting oil.

Water saturation s_w (-)	Phase (mrad)	Resistivity (ohm m)
1.0	-3.4	279.1
0.8	-4.3	449.6
0.6	-5.7	853.7
0.4	-7.6	1740.0
0.2	-14.5	9149.2

3
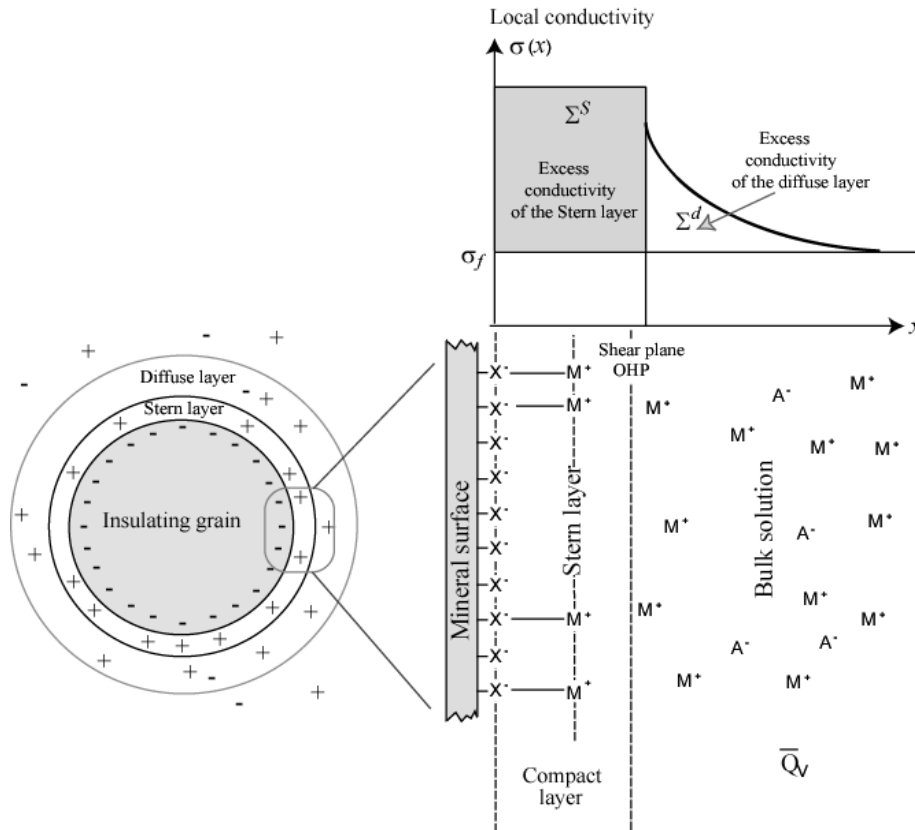
1

2

3   **Figure 1.** Sketch of the electrical double layer at the pore water interface for a fully water-saturated

4   sand. The electrical double layer is made of the Stern layer with mobile counterions able to move

5   tangentially along the mineral surface and the diffuse layer of counterions and coions existing in the

6   pore water in the vicinity of the mineral/water interface. For a pack of silica grains, the main

7   polarization mechanism seems to be associated with the polarization of the Stern layer. The

8   conductivities Σ^S and Σ^d are the specific surface conductivities (in S) of the Stern and diffuse layers,

9   respectively, and $\bar{Q}_V$ is the excess of charge of the pore water per unit pore volume at full water

10   saturation and due only to the contribution of the diffuse layer coating the surface of the pores.

a. Non-wetting oil

water silica

oil

b. Wetting oil

oil silica

water

1
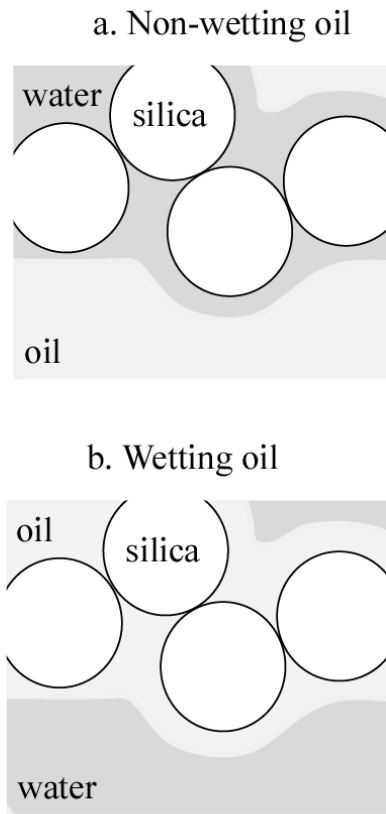
Figure 2. Sketch showing the difference in the position of the different phases between the solid

phase, oil, and the pore water depending on the wettability of the oil with respect to the solid phase

(silica). **a.** Oil is the non-wetting fluid. They are two interfaces that may carry an electrical double

layer: the solid/water interface and the oil/water interface. The electrical diffuse layer of the pore

water is squeezed in a smaller volume when the saturation of the oil phase increases. **b.** Oil is the

wetting phase.

1

2
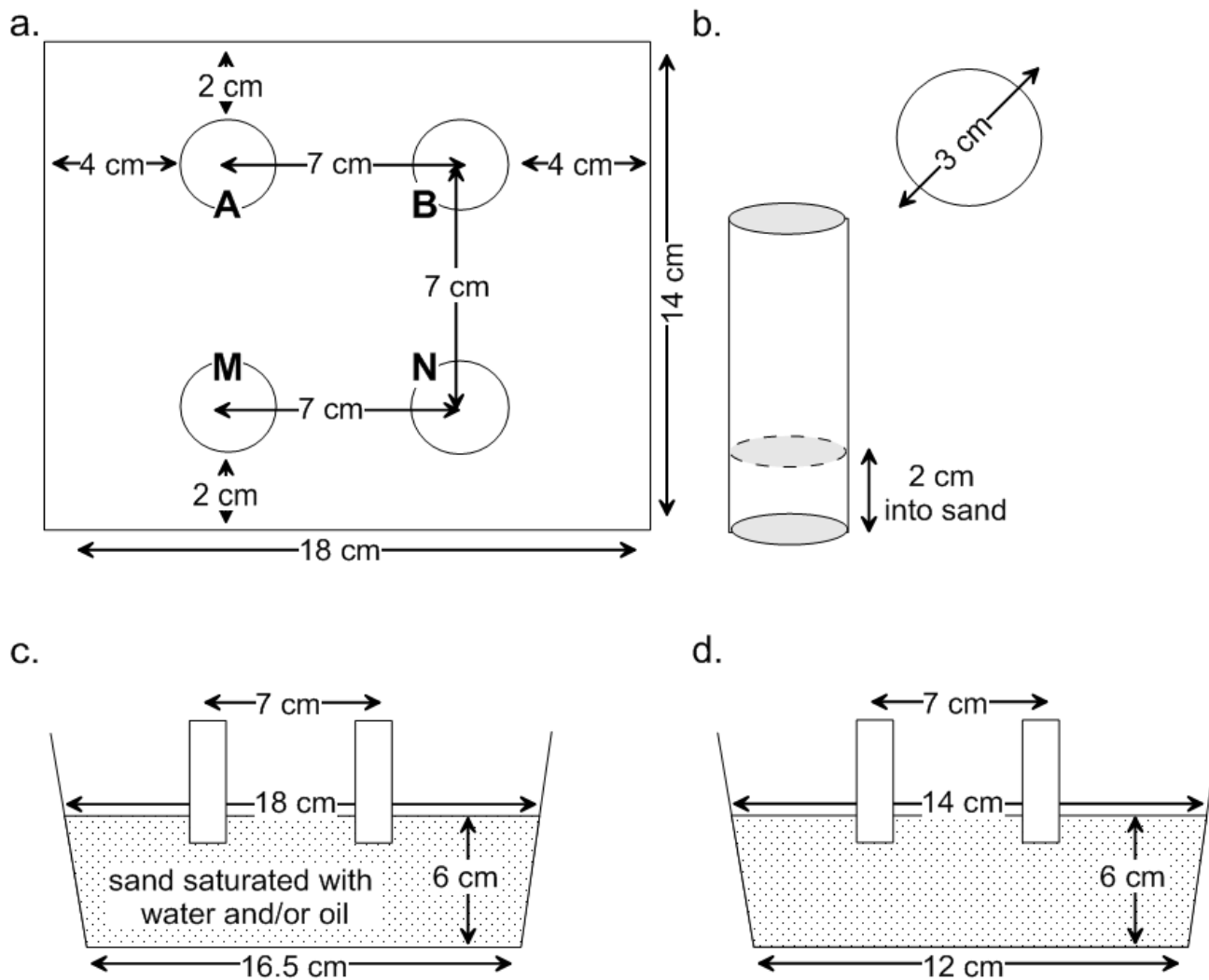
3

4

5   **Figure 3.** Sketch of the experimental setup using the Petiau Pb/PbCl$_2$ electrodes manufactured by

6   Geonesis. **a.** View of above. **b.** Size of the Petiau electrodes (from Geonesis). **c. d.** Views from the

7   side.

1

Non-wetting oil, tap water, fine sand (type A)

2
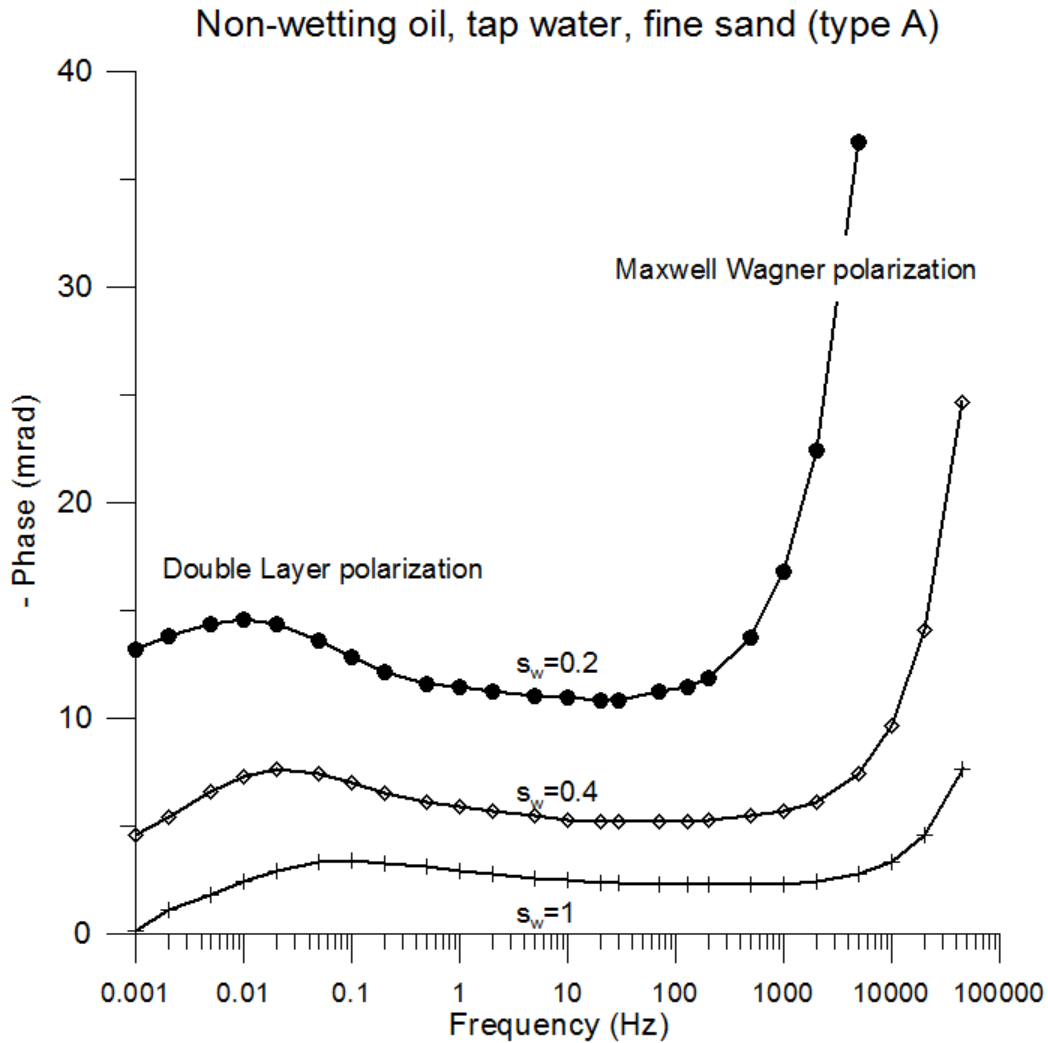
Figure 4. Full spectra of the phase shift between the current and the voltage. The low (ordinary)

frequency polarization is usually considered to be due to electrical polarization phenomena with

possibly a contribution from membrane polarization (see Vinegar & Waxman, 1984) while at higher

frequencies, the response is controlled by the Maxwell-Wagner polarization. This Maxwell-Wagner

contribution to the overall polarization is not considered in the present study.

1

2
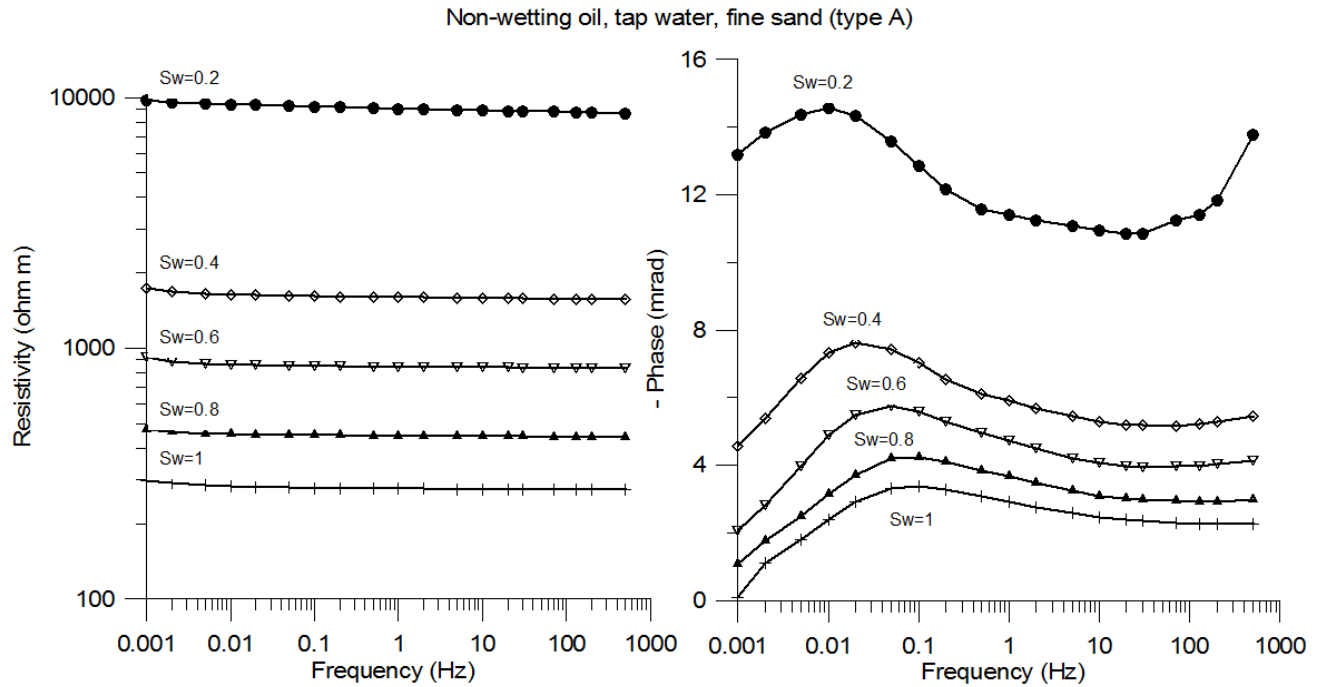
3

4

5 **Figure 5.** Modulus and phase of the complex resistivity for a non-wetting (NW) oil for different

6 values of the relative water saturations in the range 1.0 to 0.2 (the case corresponding to the fully oil

7 saturated sand could not be measured). Sand: Type A (fine sand).

1

Non-wetting oil, fine sand (type A)

tw: tap water
dw: distilled water
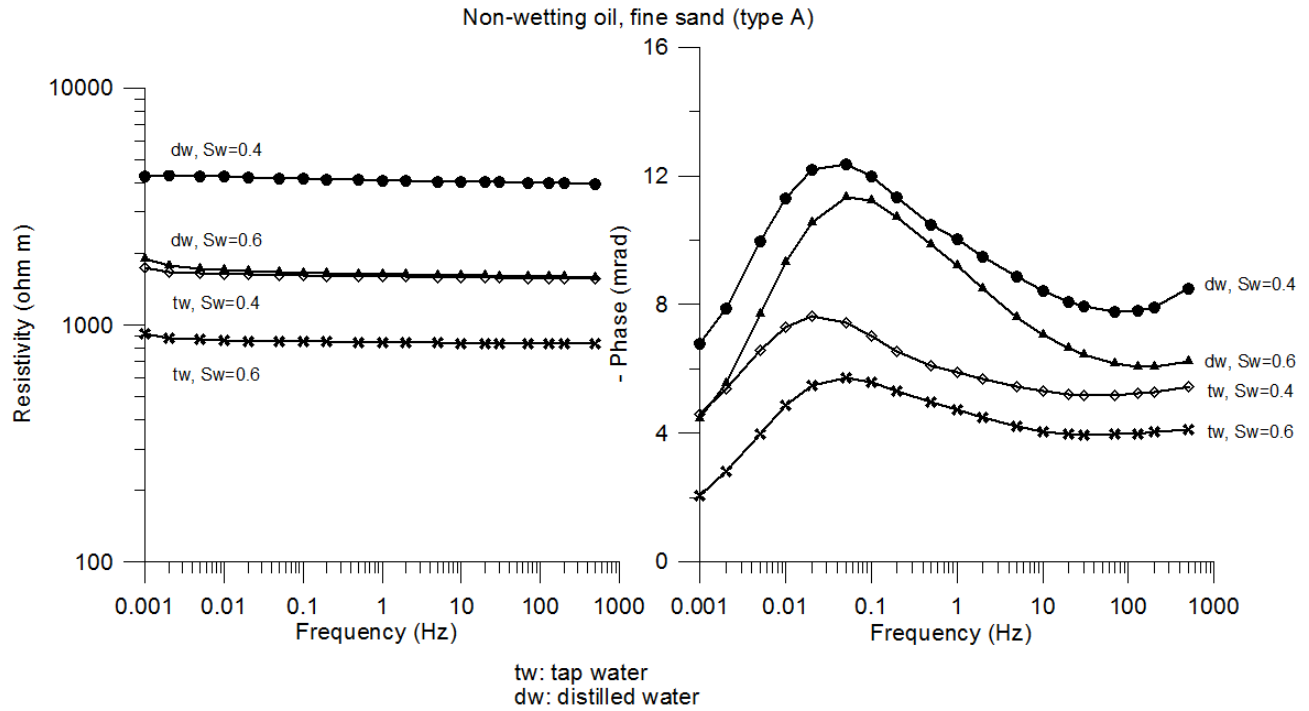
2

3

4 **Figure 6.** Modulus and phase of the complex resistivity for a non-wetting (NW) oil for two different

5 values of the water saturations $s_w = 0.6$ and $s_w = 0.4$ for two values of the conductivity of the pore

6 water. Sand: Type A (fine sand). Note that smaller is the conductivity of the pore water, higher the

7 value of the phase angle. The error bars are explicitly shown except when they are on the order of the

8 size of the symbols or smaller.

1
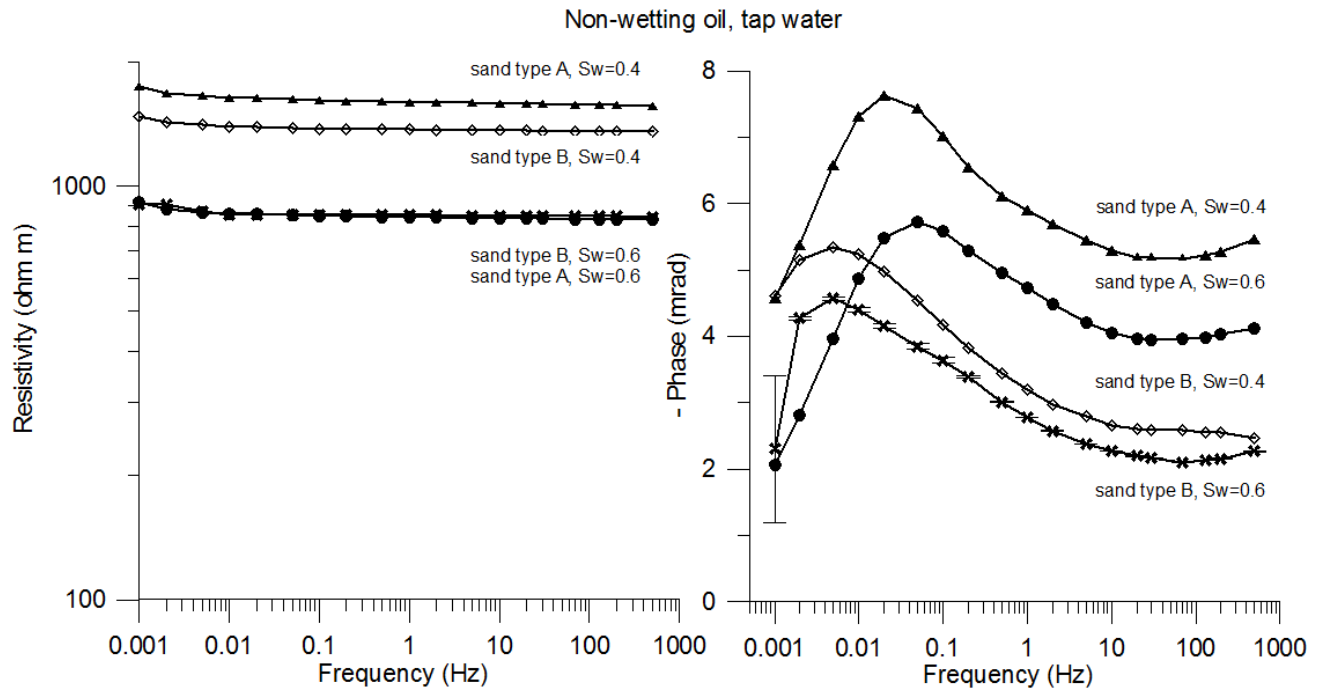
2

3

4   **Figure 7.** Modulus and phase of the complex resistivity for a non-wetting (NW) oil for two different

5   values of the water saturations $s_w = 0.6$ and $s_w = 0.4$ and for two values of the mean grain size. Sand:

6   Type A (fine sand) and Type B (coarse sand). Note that the finest sand corresponds to the highest

7   value of the absolute value of the phase angle and the highest specific surface area and surface

8   conductivity. The error bars are explicitly shown except when they are on the order of the size of the

9   symbols or smaller.

1

2
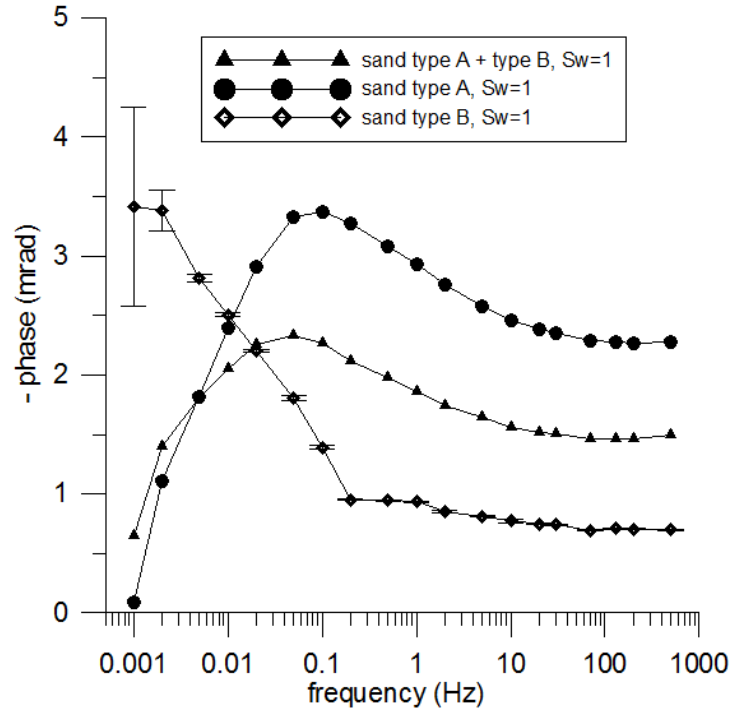
3

4 **Figure 8.** Phase of the complex resistivity for a 1:1 mixture (in volume) of sand A (fine sand) and

5 sand B (coarse sand) compared with the phase spectra for Sand A and Sand B at full water

6 saturation. The error bars are explicitly shown except when they are on the order of the size of the

7 symbols or smaller.

8
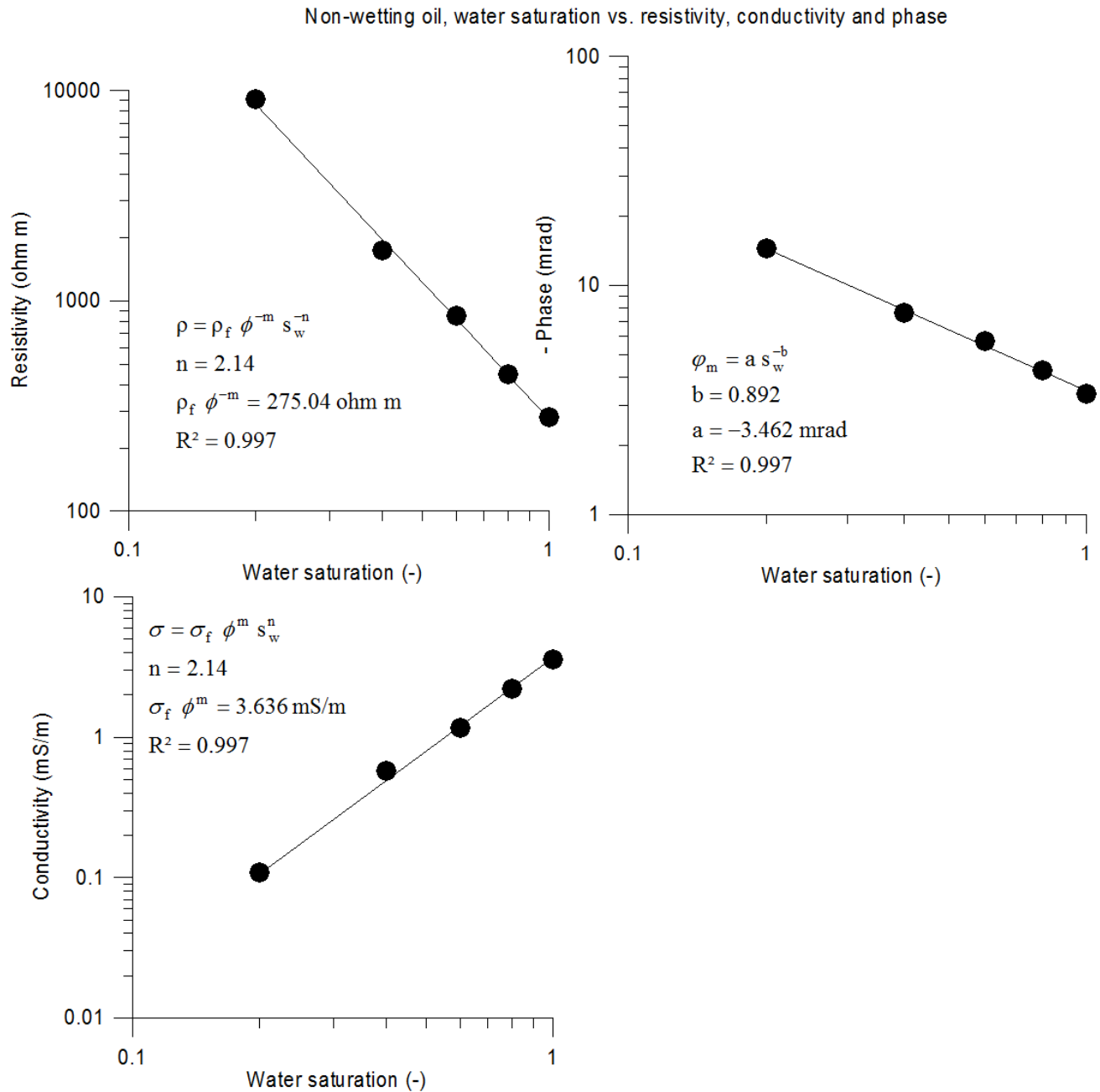
Figure 9. Modulus and peak value of the phase of the complex resistivity/conductivity for a non-wetting (NW) oil as a function of the saturation of the water phase. Type A (fine sand). The fit of the linear trend between the resistivity and the saturation provides a value for the second Archie's exponent *n* when surface conductivity can be neglected in the in phase conductivity.

1

2

Non-wetting oil, tap water, fine sand (type A)
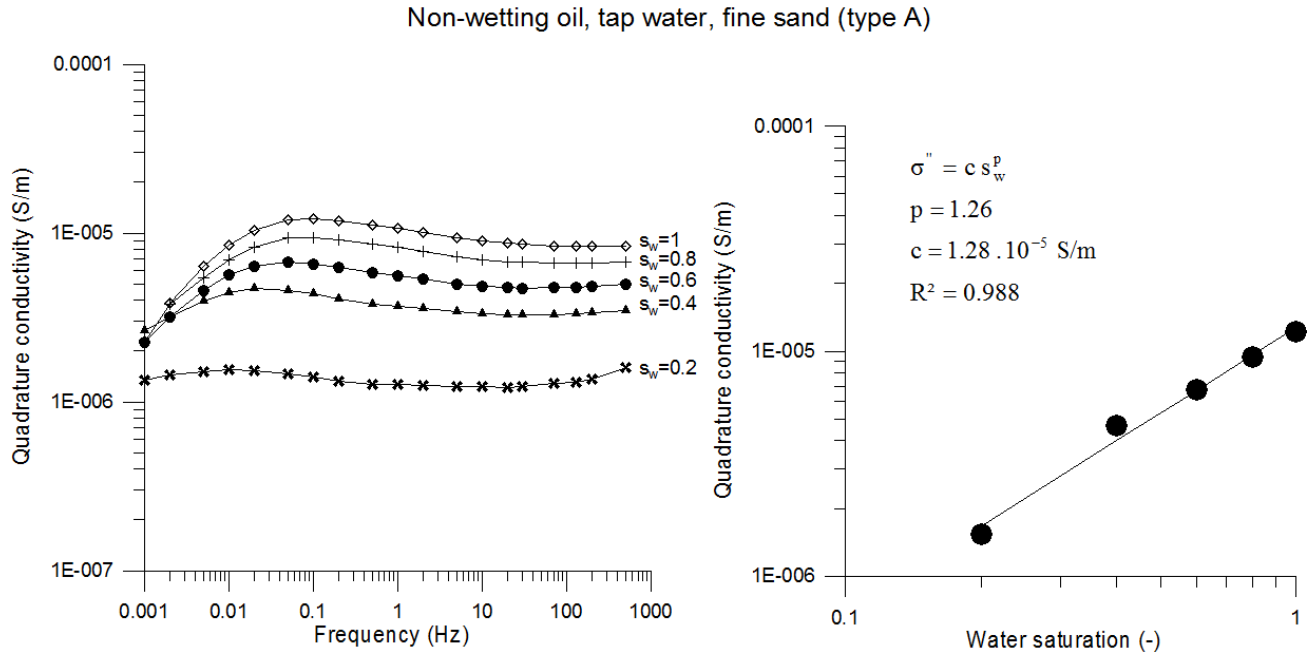
3

4

5   **Figure 10.** Left side: Quadrature or imaginary component of the complex conductivity versus the

6   ordinary frequency f. Right side: Quadrature or imaginary component of the complex conductivity

7   versus the water saturation at the frequency corresponding to the low frequency peak of the phase.

8

9
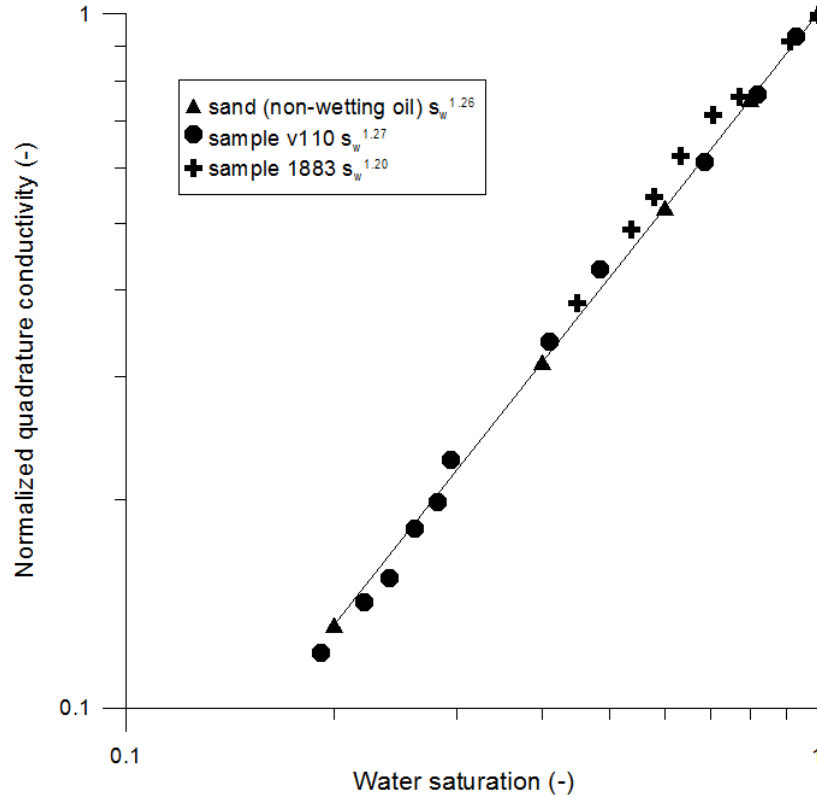
Figure 11. Quadrature (imaginary) conductivity versus water saturation. Comparison between our results for the sand filled with the non-wetting oil and the two sandstone samples investigated by Vinegar & Waxman (1984). The values reported on the figure represent the values of the exponent p (the line represents the linear trend with $p = 1.26$).